Identification of Spurious Signals from Permeable Ffowcs Williams and Hawkings Surfaces

Leonard V. Lopes*
NASA Langley Aeroacoustics Branch
Hampton, VA

D. Douglas Boyd, Jr.
NASA Langley Aeroacoustics Branch
Hampton, VA

Douglas M. Nark
NASA Langley Structural Acoustics Branch
Hampton, VA

Karl. E. Wiedemann
Analytical Services and Materials
Hampton, VA

Integral forms of the permeable surface formulation of the Ffowcs Williams and Hawkings (FW-H) equation often require an input in the form of a near field Computational Fluid Dynamics (CFD) solution to predict noise in the near or far field from various types of geometries. The FW-H equation involves three source terms; two surface terms (monopole and dipole) and a volume term (quadrupole). Many solutions to the FW-H equation, such as several of Farassat's formulations, neglect the quadrupole term. Neglecting the quadrupole term in permeable surface formulations leads to inaccuracies called spurious signals. This paper explores the concept of spurious signals, explains how they are generated by specifying the acoustic and hydrodynamic surface properties individually, and provides methods to determine their presence, regardless of whether a correction algorithm is employed. A potential approach based on the equivalent sources method (ESM) and the sensitivity of Formulation 1A (Formulation S1A) is also discussed for the removal of spurious signals.

Nomenclature

English:

a	vortex ring core radius
A	monopole source strength
$A, B, \boldsymbol{C}, \boldsymbol{D}$	directivity coefficients
c	speed of sound
$\boldsymbol{d}$	perturbation of equivalent sources
f	integration surface defined by $f = 0$
$\boldsymbol{F}$	dipole source term
J	Jacobian of surface area
$\boldsymbol{J}$	Jacobian of equivalent source pressure
$H(x)$	Heaviside function
$\boldsymbol{M}$	Mach vector
$\hat{\boldsymbol{n}}$	outward directed unit normal vector
p'	acoustic pressure
$\boldsymbol{P}$	compressive stress tensor
Q	monopole source term
R	vortex ring radius
$R(m_1, m_2)$	propagation function
r	radiation vector
r, z	spherical coordinates
s_0	distance from vortex ring origin
$\boldsymbol{S}_{eq}$	surface of equivalent sources
t	observer time
$\boldsymbol{T}$	quadrupole source term
u_1, u_2	time-independent surface coordinates
$\boldsymbol{u}, \boldsymbol{v}$	Cartesian flow and surface velocity
$\boldsymbol{V}$	forward velocity
$\boldsymbol{W}$	convection velocity of vortex ring
$\boldsymbol{x}$	Cartesian coordinates
$\boldsymbol{y}$	sample location in vortex ring frame
$\boldsymbol{y}$	monopole source location

Greek:

α	attenuation factor
Γ	vortex ring strength
$\delta(x)$	Dirac delta function
$\boldsymbol{\delta}$	Kronecker delta
Δ	difference
ε	total relative error
λ	damping factor
$\boldsymbol{\nu}$	attenuated velocity
ρ	fluid density
Σ	retarded surface
τ	source time
Φ	angle around vortex ring center axis
Ψ	stream function
ω	monopole oscillation frequency

Subscript:

$1, 1A$	Formulation 1 and 1A
a, ss	acoustic and spurious signal
eq, c	equivalent source and collocation point
e	vortex edge on core circumference
m, d, q	monopole, dipole, and quadrupole
M	point monopole noise source
r	radiation direction
ret	retarded time
s, v	surface and volume noise sources
VR	vortex ring noise source

AHS 73rd Annual Forum, Fort Worth, Texas, USA, May 9-11, 2017. *Corresponding author: **leonard.v.lopes@nasa.gov.**

VC	vortex core
Superscript:	
∞	freestream quantity
n	iteration
T	Transpose
$\bar{}$	generalized function
$'$	acoustic quantity
$\hat{}$	unit vector
Symbol:	
$\Box^2$	wave operator, $1/c_\infty^2 \partial^2/\partial t^2 - \partial^2/\partial \boldsymbol{x}_i \partial \boldsymbol{x}_j$

Background

The derivation of the FW-H equation (Ref. 1) uses generalized function theory (Ref. 2) and Lighthill's stress tensor (Refs. 3, 4) to define the acoustic pressure from a surface in arbitrary motion. Equation 1 shows the general form of the FW-H equation, which includes two surface terms, identified by the delta function operating on the surface, $\delta(f)$, and a volume term, identified by the Heaviside function operating on the surface, $H(f)$. These are the monopole, dipole, and quadrupole noise sources, respectively. Q is the monopole source term, $\boldsymbol{F}_i$ is the dipole source term, and $\boldsymbol{T}_{ij}$ is the Lighthill stress tensor. The surface f, shown in Fig. 1, can be impermeable, such as a rotor blade surface, or permeable, such as a virtual data surface surrounding the entire rotor. The permeable form of the FW-H equation is used often with a CFD solution. The CFD solution is used to resolve the near field hydrodynamics and provide the fluid properties at the permeable (ρ, $\rho \boldsymbol{u}_i$, p) and/or impermeable (p) surface. Integral forms of the FW-H equation use the fluid properties provided by the CFD solution to predict the noise at any observer location. This technique has been applied to many different types of geometries such as helicopter rotors, open rotors, landing gear, slats, flaps, trailing edges, and jets (Refs. 5–10).

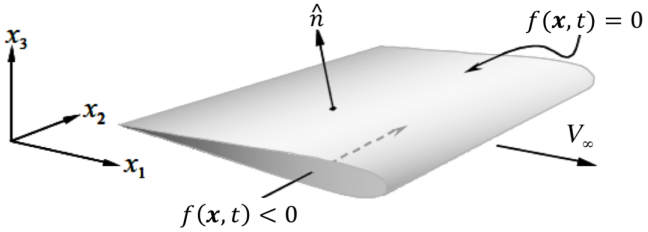

Fig. 1: Description of a surface by $f(\mathbf{x},t) = 0$, $\hat{\boldsymbol{n}}_i = \frac{\partial f}{\partial \mathbf{x}}$, $f(\mathbf{x},t) < 0$ inside, and $f(\mathbf{x},t) > 0$ outside the surface.

Permeable data surfaces are used to encapsulate noise sources and propagation effects that may be off the physical surface of the geometry. An example of this is jet mixing noise, where turbulence mixing in the jet exhaust generates noise and the jet plume influences the propagation of the noise to the far field. Noise prediction using an impermeable surface does not provide the correct result because most of the noise is generated away from the solid surface. Therefore, a volume integration would be required to predict the noise. Since solutions of the quadrupole term would require a volume integration and complex Green's function, the computational requirements are significant. If the noise sources and plume region were to be captured inside a permeable surface that surrounds the plume region, the monopole and dipole terms of the FW-H equation would include the noise from the sources and propagation effects inside the permeable data surface. This removes the need for a volume integration, significantly decreasing computation time.

Solutions of the FW-H equation, such as Farassat's Formulation 1A (Ref. 11) shown in Eq. 2 and 3, do not include volume integration terms, but instead provide both permeable and impermeable solution options. In many applications, such as the noise from a low tip-speed hovering rotor, the impermeable solution is acceptable because most noise is generated by the impermeable surface. In configurations that require a permeable solution, neglecting the quadrupole term is thought to be satisfactory because the permeable data surface encapsulates any noise sources and nonlinear propagation effects. Neglecting the quadrupole term in the permeable surface method is only valid if the quadrupole flow features are completely encapsulated inside the permeable surface. If quadrupole terms outside the permeable data surface are not negligible, then ignoring them leads to errors, which are called 'spurious signals.' These errors are the result of only a partial accounting for volume terms, those inside the penetrable data surface; whereas, volume terms outside the surface are neglected. These spurious signals can occur in many applications that employ permeable surfaces mentioned above when the permeable surface does not encapsulate all quadrupole terms. This paper will begin with a technique to identify if spurious signals are present in a noise prediction using permeable FW-H surfaces. Then two examples of the application of the technique will be provided. Finally, this paper will propose a method that can be used to negate the spurious signals using the sensitivity of the noise prediction.

$$\bar{\Box}^2 p' = \frac{\partial}{\partial t}\{Q\delta(f)\} - \frac{\partial}{\partial \boldsymbol{x}_i}\{\boldsymbol{F}_i \delta(f)\} + \frac{\bar{\partial}^2}{\partial \boldsymbol{x}_i \partial \boldsymbol{x}_j}\{\boldsymbol{T}_{ij} H(f)\} \quad (1)$$

$$4\pi p'_m(\boldsymbol{x}_i,t) = \int_{f=0} \left[(\dot{Q}J + Q\dot{J})A_{1A} + QJB_{1A} \right]_{ret} du_1 du_2 \quad (2)$$

$$4\pi c_\infty p'_d(\boldsymbol{x}_i,t) = \int_{f=0} \left[(\dot{\boldsymbol{F}}_i J + \boldsymbol{F}_i \dot{J})\boldsymbol{C}_{1A,i} + \boldsymbol{F}_i J \boldsymbol{D}_{1A,i} \right]_{ret} du_1 du_2 \quad (3)$$

$$A_{1A} = R(0,1)A_1, \qquad B_{1A} = R(0,1)\dot{A}_1, \qquad A_1 = R(1,1)$$
$$\boldsymbol{C}_{1A} = R(0,1)\boldsymbol{B}_1, \qquad \boldsymbol{D}_{1A} = R(0,1)\dot{\boldsymbol{B}}_1 + \boldsymbol{C}_1$$
$$\boldsymbol{B}_1 = R(1,1)\hat{\boldsymbol{r}}, \qquad \boldsymbol{C}_1 = c_\infty R(2,1)\hat{\boldsymbol{r}}$$
$$\boldsymbol{r} = \boldsymbol{x}(t) - \boldsymbol{y}(\tau), \qquad r = \sqrt{\boldsymbol{r}_i \boldsymbol{r}_i}, \qquad \hat{\boldsymbol{r}} = \boldsymbol{r}/r$$
$$R(m_1,m_2) = r^{-m_1}(1 - \boldsymbol{M}_i \hat{\boldsymbol{r}}_i)^{-m_2}$$

Cause of Spurious Signals

Equation 1 is the general form of the FW-H equation, where, for a permeable surface, the source terms are defined by Eqs. 4 through 6 and include the monopole, dipole, and quadrupole term, respectively. The right hand side of the FW-H equation can be classified into two types of source terms: surface and volume. The surface terms are the combination of monopole and dipole terms; the volume term is equal to quadrupole term. These are shown in Eqs. 7 and 8. The total acoustic pressure is the sum of the surface and volume pressures, $p' = p'_s + p'_v$.

$$Q = \rho_\infty \boldsymbol{v}_j \hat{\boldsymbol{n}}_j + \rho(\boldsymbol{u}_j \hat{\boldsymbol{n}}_j - \boldsymbol{v}_j \hat{\boldsymbol{n}}_j) \quad (4)$$

$$\boldsymbol{F}_i = \boldsymbol{p}_{ij}\hat{\boldsymbol{n}}_j + \rho \boldsymbol{u}_i(\boldsymbol{u}_j\hat{\boldsymbol{n}}_j - \boldsymbol{v}_j\hat{\boldsymbol{n}}_j) \tag{5}$$

$$\boldsymbol{T}_{ij} = \rho \boldsymbol{u}_i\boldsymbol{u}_j + \boldsymbol{P}_{ij} + c_\infty \rho \boldsymbol{\delta}_{ij} \tag{6}$$

$$\bar{\Box}^2 p'_s = \bar{\Box}^2 p'_m + \bar{\Box}^2 p'_d = \frac{\partial}{\partial t}\{Q\delta(f)\} - \frac{\partial}{\partial \boldsymbol{x}_i}\{\boldsymbol{F}_i\delta(f)\} \tag{7}$$

$$\bar{\Box}^2 p'_v = \bar{\Box}^2 p'_q = \frac{\bar{\partial}^2}{\partial \boldsymbol{x}_i \partial \boldsymbol{x}_j}\{\boldsymbol{T}_{ij}H(f)\} \tag{8}$$

Figure 2 shows a diagram of a source geometry causing a wake region and acoustic sources. This is a simple representation of a CFD solution that would be used as input into the FW-H equation. The freestream flow velocity is from left to right. The noise is generated by the volume displacement by the body (monopole noise), pressures on the physical surface (dipole noise), and from turbulence mixing inside the wake, as well as propagation effects (quadrupole noise). In Fig. 3, the same configuration is shown with a permeable FW-H surface that encapsulates the source geometry and a portion of the wake region near the body. The monopole and dipole noise emitted by the permeable surface replaces the noise from the sources inside the surface, including any quadrupoles and propagation effects inside, and hence the sources and wake inside are not shown in the figure. The monopole and dipole noise can be calculated by applying a free space Green's function to a surface integration over the permeable surface, such as Farassat's Formulation 1A (Ref. 11). The quadrupole noise generated outside the surface is calculated by a volume integration of the entire region outside the surface, similar to Equation 14 from Reference 12. The noise at the observer is the combination of the acoustic pressure from the permeable surface, p'_s, and from the volume, p'_v. The noise everywhere inside the surface, by definition of the generalized functions employed in the derivation of the FW-H equation, is exactly zero (i.e., if the acoustic pressure is calculated inside the surface, the sum of the surface and volume terms equates to exactly zero).

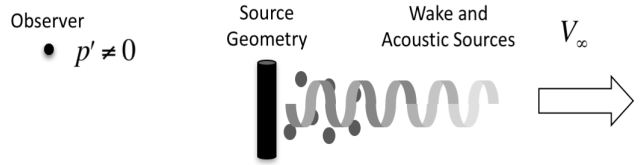

Fig. 2: Diagram of source geometry placed in uniform flow generating a wake and acoustic sources. Observer is also shown.

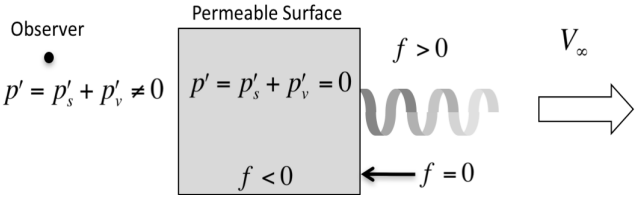

Fig. 3: Diagram of permeable surface placed around source geometry and part of the wake and acoustic sources. Noise at an observer is the combination of the surface and volume terms. p' is zero everywhere inside thee surface.

The volume term, p'_v, is computationally intensive to calculate. In many FW-H solvers, p'_v is neglected with the assumption that its contribution to the noise is small. This assumption is argued to be valid because the majority of the noise generation occurs near the body, which is inside the permeable surface. However, the FW-H equation is an exact rearrangement of the Navier-Stokes equations and includes all hydrodynamic flow and acoustic phenomena. Because the hydrodynamic flow is included in the right hand side of the FW-H equation and solutions to the FW-H equation employ a free space Green's function, the hydrodynamic wake passing through the permeable surface radiates from the surface as an acoustic wave. The volume term, when included, cancels out acoustics that radiate due to the hydrodynamics passing through the surface via Lighthill's stress tensor. When the volume term is excluded from the FW-H solution, the hydrodynamic contribution from the surface source terms are not cancelled out properly. Figure 4 shows a diagram of the case where the volume term is not included in the computation, hence the noise sources and wake outside the surface are not included in the diagram. The noise at the observer is no longer equal to the combination of the surface and volume terms. The noise inside the surface is no longer zero and is equal to only the surface terms. Becauseuse the noise inside is zero when all sources are accounted for, when the volume term is not accounted for, the noise inside is equal to the negative of the volume term that was excluded.

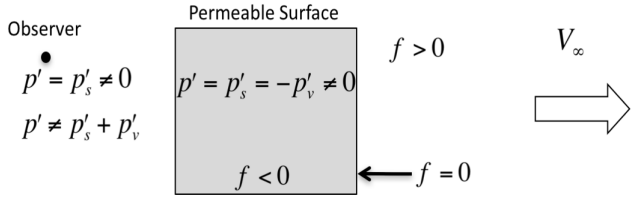

Fig. 4: Diagram of permeable surface placed around source geometry without volume term. Noise inside the surface is no longer zero and is equal to the negative of the volume term that was excluded.

The noise predicted from the surface terms includes noise from acoustic sources that are located inside the permeable surface, shown as small circles in Fig. 2 and whose noise at the observer is denoted by p'_a, and noise from flow that crosses the surface that would have been cancelled by the quadrupole term if it had been included. The noise from the permeable surface caused by the acoustic sources inside the surface is zero inside the surface and nonzero outside. The contributions from the surface that should have been cancelled by the quadrupole term are identified as spurious signals, p'_{ss}. The spurious signals, because they should have been cancelled out by the volume term, are equal to the negative of the quadrupole noise, $p'_{ss} = -p'_v = -p'_q$. This error occurs inside and outside the permeable surface, shown in Fig 5. It is also important to note that the reciprocal is also possible; i.e., if a noise source is outside the FW-H surface, it will radiate inward and be zero everywhere outside. However, this does not change the spurious signal, which will radiate inward and outward.

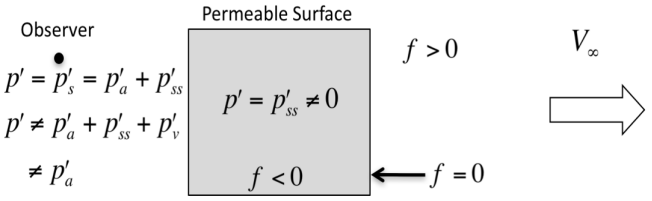

Fig. 5: Diagram of spurious signals caused by not including the quadrupole term. These occur inside and outside the permeable surface.

Without predicting the quadrupole noise, the noise outside the permeable surface contains acoustic pressure from the sources inside the surface as well as spurious signals. It is impossible to determine if the acoustic pressure predicted outside the surface contains spurious signals without knowledge of the flow field inside because the noise generation inside the surface is unknown; i.e., it is unclear whether flow phenomena on the surface are acoustic or hydrodynamic in nature. However, as the next section will show, spurious signals can be identified by predicting the noise from the permeable surface inside the surface where the noise from acoustic sources is calculated as zero. Because the spurious signals are the negative of the quadrupole noise, the nonzero noise inside the surface provides guidance to the inaccuracy incurred when ignoring the quadrupole term. If the quadrupole noise is small, the spurious signal noise inside the surface will also be small. If the noise inside the surface is large, the spurious signal noise is large and the noise predicted outside may contain large amounts of spurious signals.

In the next section, two example cases are shown that reproduce spurious signals. The examples include a cube with theoretical flow quantities and a 2-bladed rotor where the tip vortex convects through the permeable surface.

Identification of Spurious Signals

This section contains results from two example cases demonstrating the identification and behavior of spurious signals. The first example is a permeable surface in the shape of a cube. The surface terms are provided by a theoretical point monopole inside the surface and a vortex ring passing through the surface. Because the contributions on the surface from the point monopole and vortex ring are determined analytically, they can be included or excluded from the source terms on the permeable surface. The second demonstration compares the noise from a permeable surface in the shape of a 'tuna can' around a rotor and from impermeable surfaces that coincide with the rotor blades. This demonstrates a practical example where predicting the noise inside the surface can provide insight into the identification of spurious signals in the noise outside the surface.

Theoretical Flow Quantities on Cube-Shaped Permeable Surface

The first example is a permeable surface in the shape of a cube whose surface properties are determined by a stationary point monopole located at the center of the cube and a simplification of a nondeforming vortex ring that convects through a wall of the cube. Because a nondeforming vortex generates no noise, the noise prediction should only include the noise from the point monopole. However, as the previous section explained, if a noise prediction does not correctly account for flow phenomena passing through the surface, the noise from the surface would be predicted incorrectly; i.e., the vortex ring passing through the surface, if everything is not correctly accounted for, would contribute to the noise at the observer.

Figure 6 shows a schematic of the permeable surface, point monopole, and vortex ring. The ambient flow field is uniform and stationary. The flow properties on the permeable surface caused by the point monopole are determined by Eqs. 9 and 10 (Ref. 13) and are denoted with a subscript M. The flow properties on the permeable surface caused by the vortex ring are determined by an equation for the stream function, shown in Eq. 11 (Ref. 14), and do not include the motion of the vortex ring. Definition of the vortex ring strength, Γ, is provided in the Appendix. From the stream function, Eqs. 12 and 13 are used to determine velocity and acoustic pressure caused by the presence of the vortex ring, denoted with a subscript VR. The influence of the convecting motion of the vortex ring on the pressure and velocity is zero, and the acoustic density due to the vortex ring is approximated as zero everywhere (incompressible). The point monopole is located at (0,0,0.5) m, is oscillating in strength at a frequency of 2 Hz, where ω is 2π times the frequency, has a source strength A of 10 Pa·m, and exists over an observer time range of 10 seconds starting at 0 seconds with 2049 samples. Figure 7 shows a schematic of the coordinate system used to determine the fluid properties of the vortex ring, which exists over a time range and sample rate that coincides with the point monopole. Each side of the permeable surface cube contains 51^2 evenly spaced grid points where the flow from the point monopole and/or vortex ring are sampled. In this example, the fluid properties at the permeable surface will be set to those from the point monopole alone, vortex ring alone, then the combination of the point monopole and vortex ring. As stated in the previous section, if the quadrupole term is not included, we would expect true acoustic sources, such as that from the point monopole, to radiate outward from the permeable surface and be zero inside the permeable surface. Similarly, as stated in the previous section, if the quadrupole term is not included, we would expect hydrodynamics, such as that from the vortex ring, to radiate inward and outward from the permeable surface.

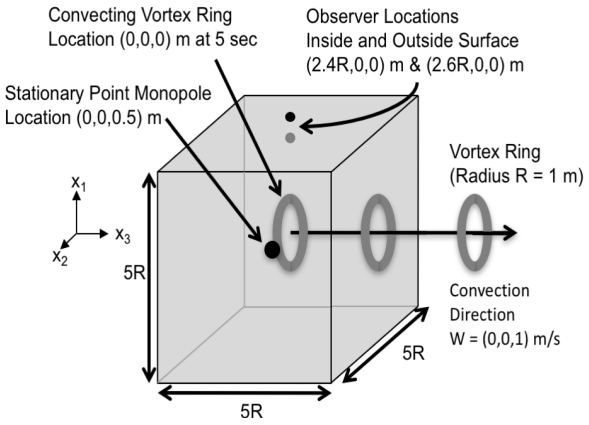

Fig. 6: Schematic of cube example problem.

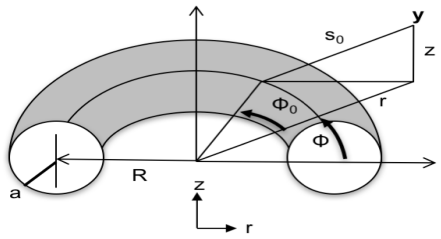

Fig. 7: Schematic of coordinate system for vortex ring (Ref. 14).

$$p'_{\mathrm{M}}(\boldsymbol{x},t)=\frac{A}{r}e^{i\omega\tau},\qquad \rho'_{\mathrm{M}}(\boldsymbol{x},t)=p'_{\mathrm{M}}/c_\infty^2 \tag{9}$$
$$\boldsymbol{r}=\boldsymbol{x}(t)-\boldsymbol{y}(\tau),\qquad r=\sqrt{r_i r_i},\qquad \hat{\boldsymbol{r}}=\boldsymbol{r}/r,\qquad t=\tau+r/c_\infty$$

$$\boldsymbol{u}_{\mathrm{M}}(\boldsymbol{x},t)=\hat{\boldsymbol{r}}\frac{\sqrt{1+(c_\infty/\omega r)^2}}{\rho_\infty c_\infty}p'_{\mathrm{M}}(\boldsymbol{x},t-\frac{1}{\omega}\tan^{-1}(c_\infty/\omega r)) \tag{10}$$

$$\Psi(\boldsymbol{y})=\frac{\Gamma R r}{4\pi}\int_0^{2\pi}\frac{\cos\Phi_0}{s_0}d\Phi_0 \tag{11}$$
$$s_0^2=z^2+r^2+R^2-2Rr\cos\Phi_0$$
$$z=\boldsymbol{y}_i\hat{\boldsymbol{k}}_i,\qquad r=\sqrt{(\boldsymbol{y}_i-z\hat{\boldsymbol{k}}_i)(\boldsymbol{y}_i-z\hat{\boldsymbol{k}}_i)}$$

$$\begin{aligned}u_{\mathrm{VR},x_1}(\boldsymbol{x},t)&=\frac{1}{r}\frac{d\Psi(\boldsymbol{x}-\boldsymbol{W}t)}{dz}\sin(\Phi),\\ u_{\mathrm{VR},x_2}(\boldsymbol{x},t)&=\frac{1}{r}\frac{d\Psi(\boldsymbol{x}-\boldsymbol{W}t)}{dz}\cos(\Phi),\\ u_{\mathrm{VR},x_3}(\boldsymbol{x},t)&=\frac{1}{r}\frac{d\Psi(\boldsymbol{x}-\boldsymbol{W}t)}{dr}\end{aligned} \tag{12}$$

$$\begin{aligned}u_{\mathrm{VR}}(\boldsymbol{x},t)&=\sqrt{\boldsymbol{u}_{\mathrm{VR},i}\boldsymbol{u}_{\mathrm{VR},i}},\\ p'_{\mathrm{VR}}(\boldsymbol{x},t)&=-\frac{1}{2}\rho_\infty u_{\mathrm{VR}}^2,\\ \rho'_{\mathrm{VR}}(\boldsymbol{x},t)&=0\end{aligned} \tag{13}$$

The first prediction is for noise emitted by the point monopole alone. The equations for a point monopole, Eq. 9 and 10, are used to determine the flow quantities on the permeable surface, which are provided as input to ANOPP2 (Ref. 15). ANOPP2 includes Farassat's Formulation 1A (F1A), which uses a free space Green's function to solve the monopole and dipole terms of the FW-H equation, called ANOPP2-F1A. ANOPP2-F1A does not include the quadrupole noise term. Figure 8(a) shows the noise prediction at the observer just inside the surface. The contribution to the total acoustic pressure from the surface terms, monopole and dipole terms, of F1A, shown in Eqs. 2 and 3, respectively, are shown and are exactly out of phase, summing to zero. This is true everywhere inside the permeable surface. The acoustic pressure caused by the point monopole directly at the inside observer is also shown. Figure 8(b) shows the prediction at the observer just outside the surface. At this observer location, the acoustic pressure from the monopole and dipole terms are no longer exactly out of phase, and the dipole term is significantly different due to the sides of the cube permeable surface cancelling; the sum of the monopole and dipole terms is no longer zero, and is similar to the acoustic pressure from the point monopole. This is true everywhere outside the surface. This example shows that as long as the noise-generating mechanisms are contained inside the permeable surface, the noise inside will be zero everywhere and outside will be nonzero. It is important to note that the cancellation of the monopole and dipole terms inside and the sum of the monopole and dipole terms being similar to the point monopole outside are strongly dependent on the spatial resolution of the permeable surfaces. It was found that the closer the observer was to the permeable surface, the higher the spatial resolution needed to be to cause an effective cancellation inside and matching outside. This is due to the surface integration technique employed in ANOPP2-F1A, which is a Riemann sum of the acoustic pressure caused by each node on the permeable surface. As mentioned by Farassat in Reference 16, a better surface integration, such as a Gauss-Legendre, would ease this limitation.

The next prediction is for a permeable surface whose flow properties are determined by the convecting vortex ring alone. Since the vortex ring is nondeforming, if all terms of the FW-H equation are included, the acoustic pressure should be zero everywhere. Figure 9(a) shows the noise prediction from the permeable surface whose flow properties are caused by only the vortex ring at the location just inside the cube. The noise predictions in Fig. 9(a) are not zero and, hence, suggest spurious signals are present. Figure 9(b) shows the noise prediction from the permeable surface whose flow properties are caused by only the vortex ring at the location just outside the cube. The predictions are not zero and are very similar to the results shown in Fig. 9(a). This coincides with the previous statement: that hydrodynamics that pass through the surface do not obey the rules outlined by the generalized functions employed in the derivation of the FW-H equation.

Figures 10 shows ANOPP2-F1A predictions from a surface whose properties are determined by the vortex ring and the point monopole. The noise at the inside observer is the same as the vortex alone, and the noise outside is the sum of the monopole and vortex ring alone cases. This shows

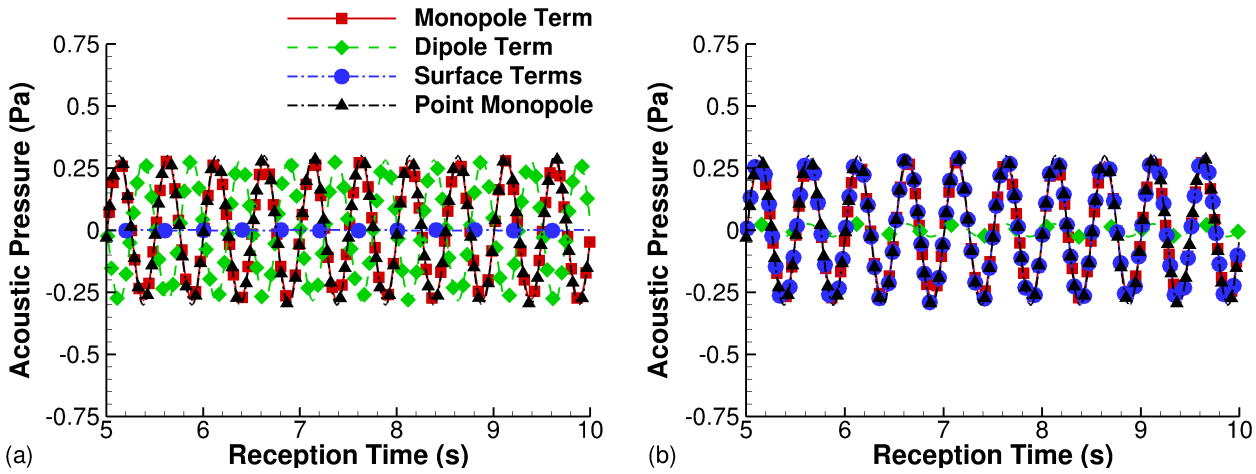

Fig. 8: ANOPP2-F1A prediction of noise from permeable surface whose flow properties are determined by the point monopole. (a) Observer is just inside the surface. (b) Observer just outside the surface.

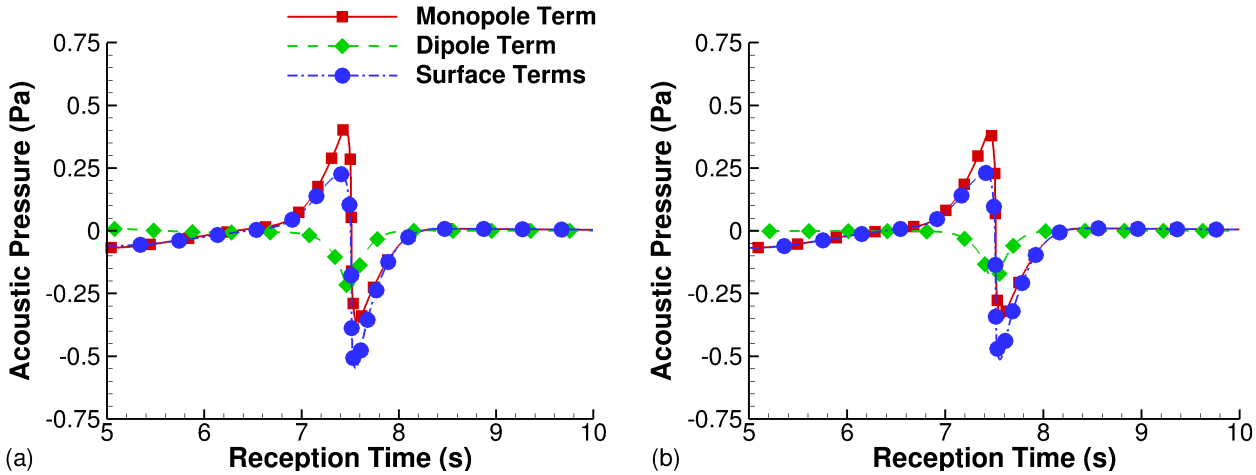

Fig. 9: ANOPP2-F1A prediction of noise from permeable surface whose flow properties are determined by the vortex ring. (a) Observer is just inside the surface. (b) Observer just outside the surface.

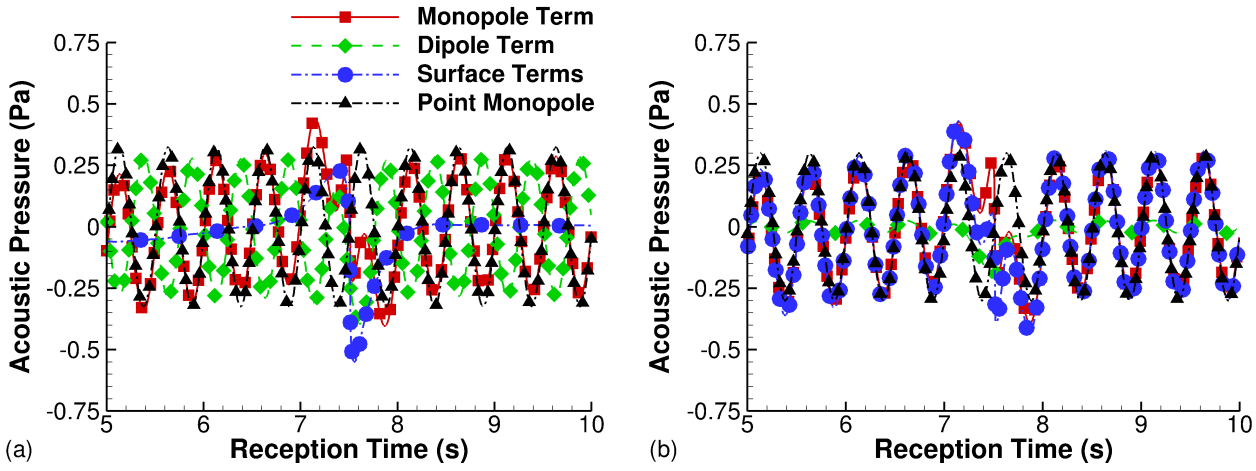

Fig. 10: ANOPP2-F1A prediction of noise from permeable surface caused by the vortex ring and monopole source. (a) Observer is just inside the surface. (b) Observer just outside the surface.

that hydrodynamic flow phenomena passing through the surface cause spurious noise inside and outside the surface while acoustic sources contained inside the surface radiate only outside the surface.

In addition to a single point, contours of acoustic pressure inside the permeable surface can be calculated to see the influence of spurious signals. Figure 11 shows a contour of acoustic pressure on a plane normal to the x_1 axis inside the cube-shaped permeable surface whose flow properties are defined by the point monopole and vortex ring. The grid inside consists of 24^2 evenly spaced observer locations ranging from -2.4 m to 2.4 m in the x_2 and x_3 axis directions centered at the origin. The range was chosen because, as mentioned before, the closer the observers to the permeable surface, the finer the permeable surface grid resolution required to accurately capture the cancellation from the point monopole. Figure 11(a) shows the acoustic pressure at an observer time of 5 seconds, when the vortex ring is in the center of the permeable surface. Notice that there is no sign of acoustic pressure from the point monopole. Figures 11(b) through 11(d) show the acoustic pressure at different observer times as the vortex passes through the permeable surface. Figure 11(f) shows the acoustic pressure as the vortex has passed fully through the permeable surface.

The next example shows that performing a similar calculation on a realistic configuration where the acoustic and hydrodynamic properties cannot be so easily separated can provide identification of spurious signals.

CFD Extracted Flow Quantities on Tuna Can-Shaped Permeable Surface

For the case of a low tip-speed hovering rotor, the impermeable formulation of the FW-H equation without the quadrupole term is expected to give acceptable results because the quadrupole noise source is minimal; i.e., the near field does not contain any acoustic sources, and the propagation of noise through the nonuniform medium is not significantly different than through a uniform medium. In this next example, a CFD computation of a two bladed hovering rotor is used to populate permeable and impermeable surfaces, which are then fed to ANOPP2-F1A for use in Farassat's Formulation 1A to predict the noise at an observer. Since the impermeable formulation without the quadrupole term is expected to give acceptable results, comparing the noise from the impermeable and permeable surface provides an estimate of the inaccuracy caused by the spurious signals. The comparison is only an estimate because a prediction using the permeable surface includes any dissipation of the acoustic waves as they propagate from the blade surface to the permeable surface, as well as the aforementioned propagation effects; however, these are assumed small compared to any spurious signals that may be present. Figure 12 shows a schematic of the rotor setup. The impermeable surfaces are the physical, rigid, 1 meter long blade surfaces, and the permeable surfaces are in the shape of a 'tuna can' around the entire rotor. The radius of the permeable surface is 1.125 m, and the height is 0.7 m. The observer locations are in the shape of a square 4 m by 4 m located 1.5 m below the lower surface of the permeable surface and contain 101^2 evenly spaced observer nodes. The conditions on the permeable and impermeable surfaces are provided by an OVERFLOW2 (Refs. 17, 18) computation which performs a fourth order in space, second order in time numerical solution to the Unsteady Reynolds-Averaged Navier-Stokes (URANS) equations using a Spalart-Allmaras turbulence model (Ref. 19). The computational method presented here is similar to that presented in Reference 20, except that because the rotor is rigid and the collective pitch is fixed, only OVERFLOW2 is necessary. That is, no coupling with a structural dynamics code was required. The computation contains 80 million points with an inner body around the rotor of radius 1.1 times the rotor radius and height of 4.5 times the rotor radius. The off body grid is uniform with grid resolution of 0.1 times the blade chord. The blades are NACA 23012 airfoil cross sections at 5 degree collective pitch. OVERFLOW2 was run for 10 revolutions before sampling for the impermeable and permeable surfaces was initiated.

Figure 13 shows ANOPP2-F1A predictions of pressure at the observer surface at a single instant in time from the impermeable (a) and permeable surfaces (b), including the difference (c), Δ, and relative error (d), ε, using Eqs. 14 and 15, respectively. The permeable surface, due to the propagation speed of acoustic waves through the CFD domain, adds a time delay which exacerbates the relative error; however, the error due to spurious signals can clearly be identified. The predictions show that the permeable surface predictions contain much higher acoustic pressure than the impermeable surfaces due to spurious signals.

$$\Delta = p'_{\text{permeable}} - p'_{\text{impermeable}} \tag{14}$$

$$\varepsilon = \frac{|p'_{\text{impermeable}} - p'_{\text{permeable}}|}{|p'_{\text{impermeable}}| + |p'_{\text{permeable}}|} \tag{15}$$

Spurious signals can be identified in Fig. 13 because predictions using the impermeable surface can provide acceptable pressures. If the noise prediction from the impermeable surface is not acceptable (i.e., if the tip Mach number is higher) then using the knowledge that the noise predicted inside will not be zero can be used to identify if spurious signals are present. The noise from the permeable surface around the rotor contains wakes passing through it. Furthermore, the quadrupole term is not accounted for, and therefore, spurious signals inside the surface are expected. Figures 14(a) through (e) shows ANOPP2-F1A predictions of noise at 5 slices through an unstructured volume of observers (19781 observer nodes) placed inside the permeable surface. Toward the bottom of the permeable surface, $x_3 = -0.35$ m, the prediction shows a high gradient of acoustic pressure toward the outer radius of the permeable surface. This is due to the tip vortex passing through the permeable surface. The noise toward the center is near zero due to the minimal wake passing through the surface near the center. The slices through the volume toward the middle of the permeable surface, $\boldsymbol{x}_i = (0.175, 0.0, -0.175)$ m, do not have spurious signal strengths as large as near the permeable surface because they are further away from the tip vortices passing through the bottom surface. However, the values of acoustic pressure are still

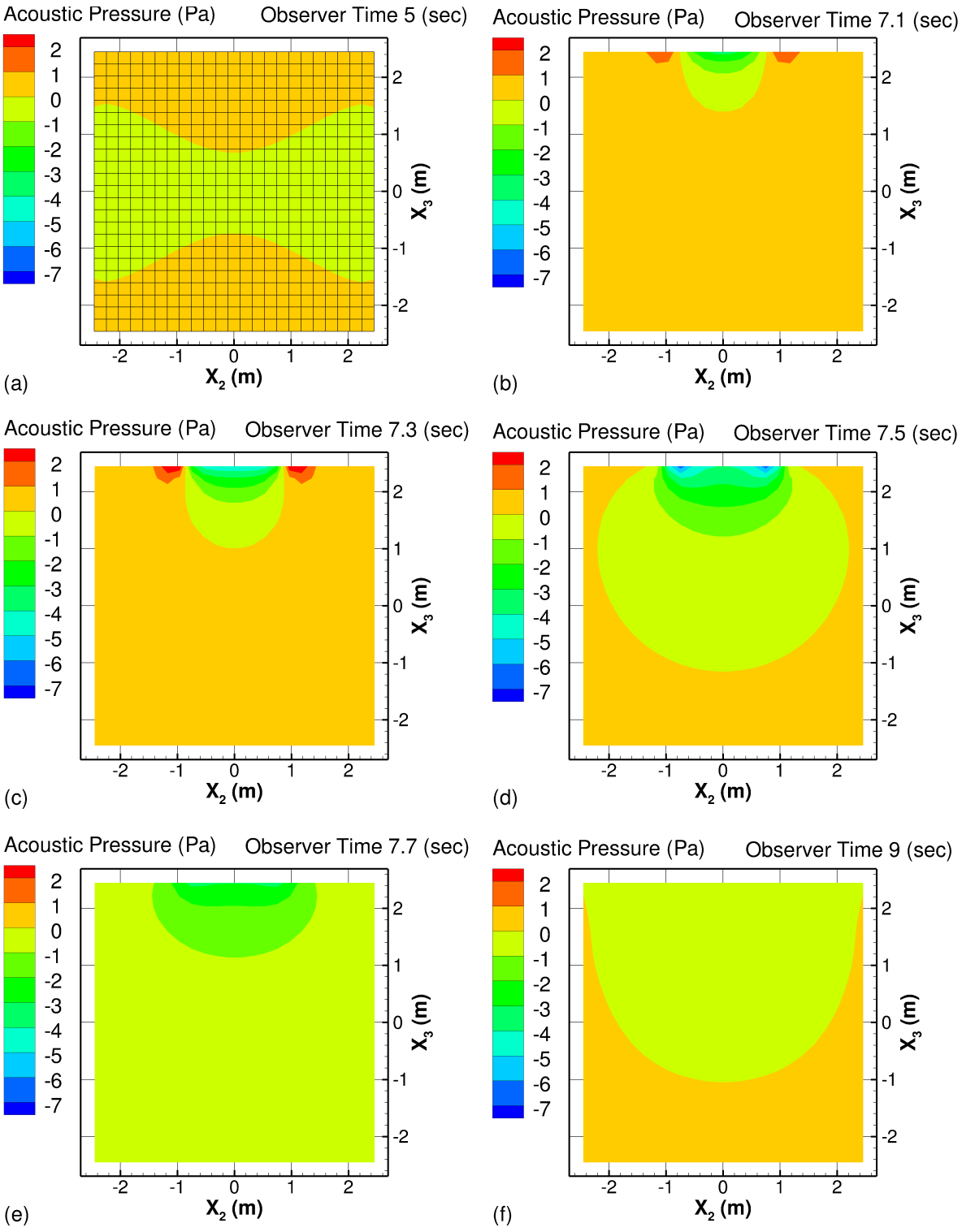

Fig. 11: Contours of acoustic pressure inside permeable surface whose properties are defined by point monopole and vortex ring. (a) through (f) show different instances of observer time. a) also shows the grid of observer locations.

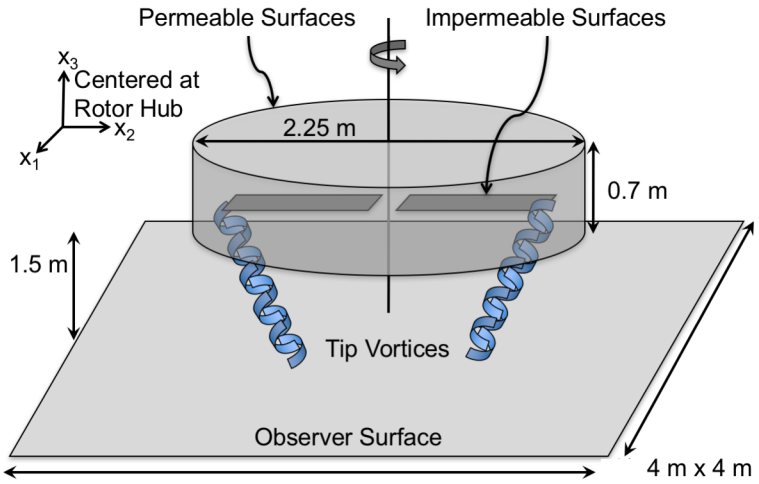

Fig. 12: Schematic of 2-bladed rotor prediction setup.

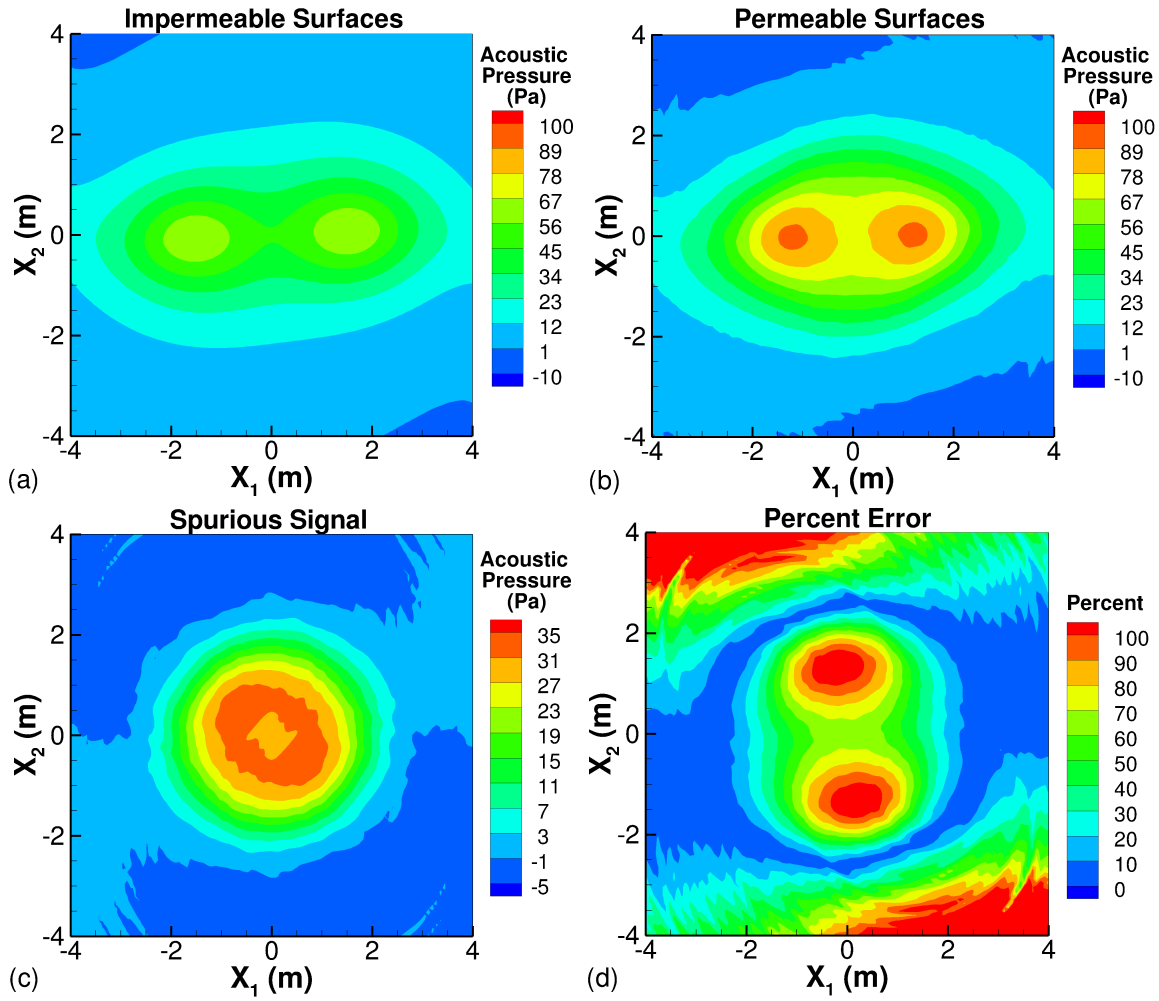

Fig. 13: ANOPP2-F1A predictions of instantaneous acoustic pressure from impermeable (a) and permeable (b) surfaces. (c) Δ as defined by Eq. 14. (d) Percent error defined as $100 * \varepsilon$ where ε is defined by Eq. 15.

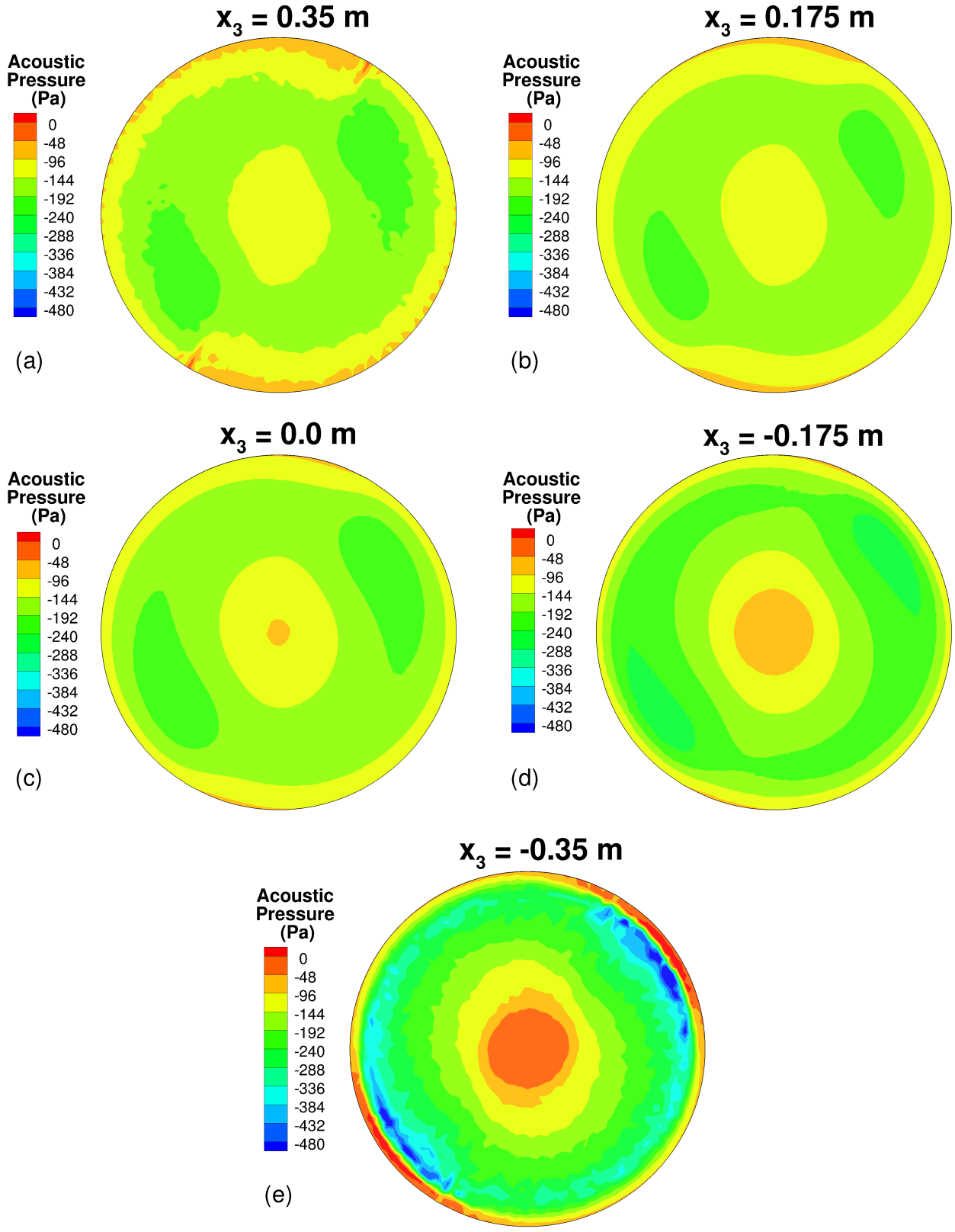

Fig. 14: ANOPP2-F1A predictions of acoustic pressure inside the tuna can-shaped permeable surface.

high due to the proximity of the observers to the permeable surface. Toward the top of the permeable surface, $x_3 = 0.35$ m, the spurious noise is caused by the inflow of the rotor. As the fluid velocity passes through the surface, this causes spurious signals. Here we see that predicting the noise on the inside of the permeable surface has provided us a way to identify if spurious signals are present.

ANOPP2-F1A provides a diagnostic tool that communicates the source terms on the surface in retarded time, called the $\Sigma-$surface, which derives its name from Formulation 3 of Farassat (Ref. 11), that contribute to the pressure at a single observer location and time. Figure 15 shows the $\Sigma-$surface for an observer located at $(0.0, 1.8, 0.0)$ m, inside the permeable surface, at the peak noise observer time, with contours of the sum of monopole and dipole noise. The upper and lower surfaces are both shown. The $\Sigma-$surface shows that the sources of noise at the observer located inside the permeable surface are from the tip vortex passing through the bottom of the surface and the flow through the top of the surface. Figure 15(a) shows a highlighted area where noise from the upper surface is contributing to the observer; this is indicative of the true acoustic source, and a surface integral of just the true acoustic source's influence on the surface would integrate to zero, similar to the previously shown monopole in cube example. Figure 15(b) shows a highlighted area where a noise source is caused by the tip vortex passing through the lower surface. This shows again that predicting noise on the inside of the permeable surface can identify when spurious signals may be contaminating the noise prediction.

Removal of Spurious Signals

In realistic situations, calculation of acoustic pressure caused by the quadrupole term of the FW-H equation is not possible due to the size of the numerical calculation that would be required to accurately capture the complete influence of the quadrupole term. Therefore, an algorithm is needed that uses only the knowledge of the behavior of spurious signals to negate any nonacoustic sources. An approach was proposed by Lockard and Casper (Ref. 21) for airframe noise prediction by applying a frequency domain, frozen gust assumption at low Mach numbers (around Mach number 0.2). Agreement was acceptable for some test cases but failed to correct for spurious signals due to a wake induced by flow over a cylinder passing through a permeable surface. Another correction method is to completely ignore portions of a permeable surface, typically downstream, where wakes are known to pass through. However, this also means that true acoustic waves on the downstream permeable surface are also ignored. Figure 16 shows predictions of acoustic pressure similar to those shown in Fig. 10 but with the side of the cube where the vortex passes through removed. The figures show that although the influence of the vortex ring is dampened, the acoustic pressure from the surface terms on the 'outside' no longer match the point monopole. Similarly, 'inside' the surface, the acoustic pressure from the surface terms is still nonzero. A third approach is to average the flow properties on the downstream direction in the frequency domain (Ref. 22). Because the convection velocity of the hydrodynamics is slower than the acoustics, averaging allows separation of the phenomena. While averaging has been shown to work for some jet noise predictions, it is not a general purpose solution, because the surface is required to be stationary or in uniform motion. Also, the technique of averaging suffers from the question of which surfaces to use. Despite multiple studies on the approach, it is still unclear when to average and what surfaces to average. Clearly, given all the research performed on addressing spurious signals for certain applications, a more robust, fundamental correction approach is needed that does not suffer from the above limitations.

In the current effort, before an algorithm can be proposed, a few constraints are defined that coincide with those imposed by Farassat on his solutions to the FW-H equation. Farassat (Ref. 23) proposed that any general solution to the FW-H equation satisfy the following constraints, which are taken verbatim from Reference 23:[1]

1. There must be no restrictions on the geometry of the noise generator (blades, airframe, etc.). This means that results for a flat (infinitely thin) plate are not acceptable.

2. There must be no restrictions on the kinematics of the noise generator. This means that the motion of the source cannot be restricted to lie on a straight line or a helicoidal surface.[2]

3. The result must be valid in the near and far fields.

4. One should be able to calculate the noise for an observer that is stationary in the medium, or in motion with the aircraft.

Noise from spurious signals cannot be separated from that of true acoustic sources outside the permeable surface; however, inside the permeable surface, true acoustic sources located inside the permeable surface generate no noise. Any predictions of noise made within the permeable surface, therefore, are from only spurious signals. The authors propose a method that leverages this behavior of spurious signals and is based on the equivalent source method (ESM) (Refs. 25, 26) and sensitivity of Formulation 1A, called Formulation S1A (Ref. 27). Figure 17 shows a schematic of an approach that uses equivalent sources on the permeable surface (surface of equivalent sources). These equivalent sources, which consist of pressure, momentum, and density at every grid point and time step of the original permeable surface, can potentially be tailored to produce an acoustic field that cancels any noise within the surface at a series of collocation points, $\boldsymbol{p}'_c$, similar to the observers shown in Fig. 11. If the surface of equivalent sources, $\boldsymbol{S}_{eq}$, is tailored such that it cancels the flow field

[1] An exception is Formulation 1B of Casper and Farassat[24] that failed to satisfy requirement 1 because of the application of a flat plate assumption. However, a more robust implementation that satisfied the requirements was proposed by Farassat and Casper in Formulation 2B[23].

[2] In addition to constraint 2, the authors add that the surface may be rigid or deforming.

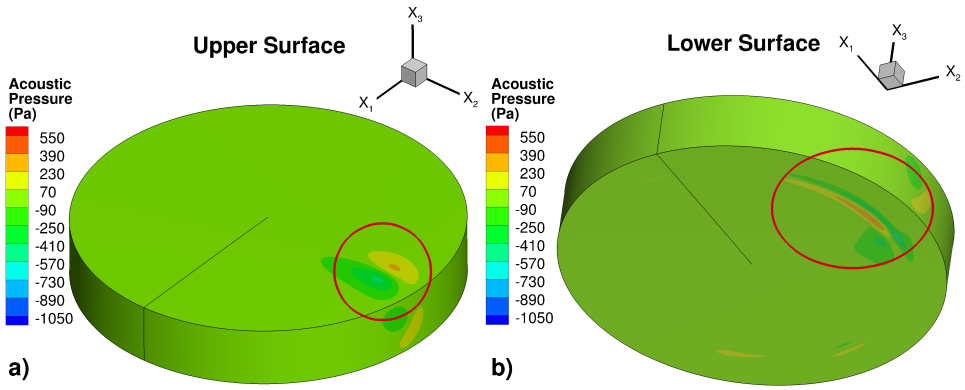

Fig. 15: $\Sigma-$surface at observer location $(0.0, 1.8, 0.0)$ m at peak noise observer time. Noise is caused from vortex passing through bottom of permeable surface and from flow through the top of the surface.

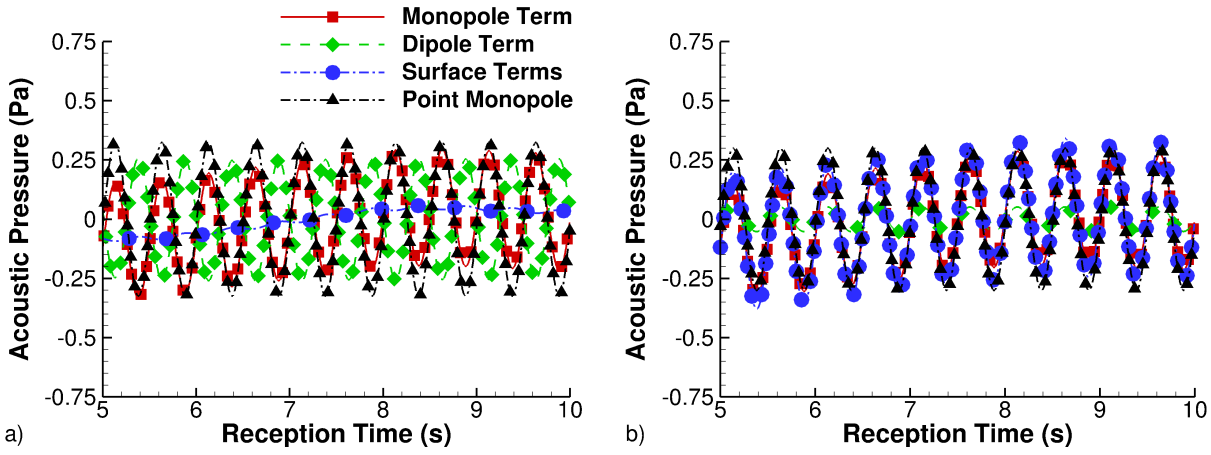

Fig. 16: ANOPP2-F1A prediction of noise from permeable surface caused by the vortex ring and monopole source using 5 of the 6 sides of the cube. (a) Observer is just inside the closed surface. b) Observer just outside the closed surface.

caused by only the hydrodynamics passing through the surface, then the noise within the permeable surface would cancel the spurious signals ($\boldsymbol{p}'_{eq} = -\boldsymbol{p}'_c = -\boldsymbol{p}'_{ss}$), and the sum of the noise outside from the permeable surface and from the surface of equivalent sources would be those from only true acoustic sources, $p' = p'_a + p'_{ss} + p'_{eq} = p'_a$. It is important to note that this does not reproduce the quadrupole term, i.e., any noise generated outside the surface is not reproduced;[3] the surface of equivalent sources merely cancel the spurious signals. Other than the size of the proposed computation for realistic problems, the challenge with this approach is that it is an ill-posed problem; there are more equations than unknowns and potentially more than one configuration to the equivalent sources that satisfy the condition. This is not unlike other problems that employ the ESM, such as beamforming, which have achieved great success regardless.

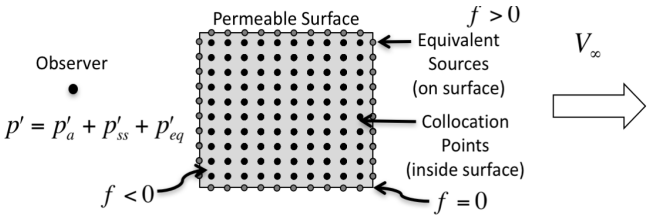

Fig. 17: Schematic of equivalent source method proposed for the correction of spurious signals.

Ultimately, we wish to solve the system of equations, shown in Eq. 16, where: $\boldsymbol{p}'_c$ is the acoustic pressure at each collocation point at every time step from the permeable surface, $\boldsymbol{p}'_{eq}$ is the acoustic pressure at each collocation point at every time step from the surface of equivalent sources, $\boldsymbol{S}_{eq}$ is the surface of equivalent sources defined at every location on the permeable surface and every time step, and [F1A] is the matrix representation of the numerical implementation of Farassat's Formulation 1A. The authors propose solving this system of equations via the Levenberg-Marquardt algorithm (Refs. 28, 29) that utilizes the Jacobian of the pressure with respect to the surface quantities, which can be provided by Formulation S1A, denoted as $\mathbf{J}$. This is shown in Eq. 17, where S is the sum of the squares to be minimized, superscript n denotes iterations, and m denotes observer time and space indices. $\boldsymbol{d}$ is the perturbation of $\boldsymbol{S}_{eq}$ between iteration and is determined by setting the derivative of S with respect to $\boldsymbol{d}$ to zero, which leads to Eq. 18, where λ is a damping factor. Implementation and application of this approach is left for future work. It is suggested that this method be tested by applying the technique to the fundamental problems demonstrated in this work.

$$-\boldsymbol{p}'_c = \boldsymbol{p}'_{eq} = [\text{F1A}]\boldsymbol{S}_{eq}, \qquad \boldsymbol{J} = \partial \boldsymbol{p}'_{eq}/\partial \boldsymbol{S}_{eq} \tag{16}$$

$$S^{n+1}(\boldsymbol{S}^n_{eq} + \boldsymbol{d}^n) \approx \sum_{i=1}^{m} (-p'_{c,i} - p'^n_{eq,i} - \boldsymbol{J}^n_i \boldsymbol{d}^n)^2 \tag{17}$$

[3]Because true acoustic sources outside the permeable surface propagate on the inside, the surface of equivalent sources would reproduce the flow quantities caused by those sources. However, the surface of equivalent sources would not propagate outside the surface and, therefore, would not reproduce the influence of the quadrupole term.

$$[\boldsymbol{J}^{\mathrm{T}}\boldsymbol{J} + \lambda \,\mathrm{diag}(\boldsymbol{J}^{\mathrm{T}}\boldsymbol{J})]\boldsymbol{d}^{n+1} = \boldsymbol{J}^{\mathrm{T}}(-\boldsymbol{p}'_c - \boldsymbol{p}'^n_{eq}) \tag{18}$$

Conclusion

This paper explored the concept of spurious signals, explained how they are generated, and provided a method to identify if they are present. Two examples were shown that demonstrate the presence of spurious signals in the prediction of acoustic pressure that utilize a permeable FW-H surface. The first example used a theoretical point monopole and a convecting vortex ring to determine the fluid properties on a permeable surface. It was shown that true acoustic sources inside the permeable surface radiate noise only outside the surface; predictions of noise inside the permeable surface result in zero acoustic pressure. It was also shown that hydrodynamic flow features passing through the permeable surface, such as that from a vortex ring, radiate noise inside and outside the permeable surface. A second example, that from a CFD computation for a hovering rotor, showed that predicting the noise inside the surface can provide insight into the potential contamination of the noise prediction outside the permeable surface due to spurious signals. Finally, a potential approach based on the equivalent source method (ESM) and the sensitivity of Formulation 1A (Formulation S1A) for the removal of spurious signals was also discussed.

References

[1]Ffowcs Williams, J. E. and Hawkings, D. L., "Sound Generated by Turbulence and Surfaces in Arbitrary Motion," *Philosophical Transactions of the Royal Society*, Vol. 264, No. 1151, 1969, pp. 321–342.

[2]Gel'fand, I. M. and Shilov, G. E., *Generalized Functions: Properties and Operations*, Vol. 1, Academic Press, Inc., 11 Fifth Avenue, New York, New York, 1964, Translated by Eugene Saletan, Department of Physics, Northeastern University, Boston, Massachusetts.

[3]Lighthill, M. J., "On Sound Generated Aerodynamically, I: General Theory," *Proceedings of the Royal Society. A, Mathematical, Physical, and Engineering Sciences*, Vol. 211, 1952, pp. 564–587.

[4]Lighthill, M. J., "On Sound Generated Aerodynamically, II: Turbulence as a Source of Sound," *Proceedings of the Royal Society. A, Mathematical, Physical, and Engineering Sciences*, Vol. 222, 1954, pp. 1–32.

[5]Morgans, A. S., Karabasov, S. A., Dowling, A. P., and Hynes, T. P., "Transonic Helicopter Noise," *AIAA Journal*, Vol. 43, No. 7, 2005, pp. 1512–1524.

[6]Spalart, P. R., Travin, A. L., Shur, M. L., and Strelets, M. K., "Initial Noise Predictions for Open Rotors Using First Principles," 16th AIAA/CEAS Aeroacoustics Conference, AIAA Paper No. 2010-3793, June 2010.

[7]Lockard, D. P., Khorrami, M. R., and Li, F., "Aeroacoustic Analysis of a Simplified Landing Gear," 10th AIAA/CEAS

Aeroacoustics Conference, AIAA Paper No. 2003-3111, May 2004.

[8]Khorrami, M. R., Singer, B. A., and Bekman, M. E., "Time-Accurate Simulations and Acoustic Analysis of Slat Free-Shear Layer," 7th AIAA/CEAS Aeroacoustics Conference, AIAA Paper No. 2001-2155, May 2001.

[9]Wolf, W. R. and Lele, S. K., "Trailing Edge Noise Predictions Using Compressible LES and Acoustic Analogy," 17th AIAA/CEAS Aeroacoustics Conference, AIAA Paper No. 2011-2784, June 2011.

[10]Lyrintzis, A. and Uzun, A., "Integral Techniques for Jet Aeroacoustics Calculations," 7th AIAA/CEAS Aeroacoustics Conference, AIAA Paper No. 2001-2253, May 2001.

[11]Farassat, F., "Theory of Noise Generation from Moving Bodies with an Application to Helicopter Rotors," NASA TR R-451, NASA Langley, 1975.

[12]Farassat, F. and Brentner, K. S., "The Uses and Abuses of the Acoustic Analogy in Helicopter Rotor Noise Prediction," AHS Specialists' Meeting on Aerodynamics and Acoustics, Feb 1987.

[13]Dowling, A. P. and Ffowcs Williams, J. E., *Sound and Sources of Sound*, Ellis Horwood Publishers, Chichester, West Sussex, England, 1983.

[14]Lugt, H. J., *Introduction to Vortex Theory*, Vortex Flow Press, Potomac, Maryland, USA, 1998.

[15]Lopes, L. V. and Burley, C. L., "ANOPP2 User's Manual," Tech. Rep. NASA/TM-2016-219342, NASA Langley, 2016.

[16]Farassat, F., "Derivation of Formulations 1 and 1A of Farassat," NASA TM 2007-214853, NASA Langley, 2007.

[17]Buning, P. G., *OVERFLOW User's Manual, Version 1.8ab*, NASA Langley Research Center, Hampton, VA, July 2003.

[18]Nichols, R., Tramel, R., and Buning, P., "Solver and Turbulence Model Upgrades to OVERFLOW2 for Unsteady and High-Speed Applications," AIAA 36th Fluid Dynamics Conference, AIAA Paper No. 2006-2824, June 2006.

[19]Spalart, P. and Allmaras, S., "A One-Equation Turbulence Model for Aerodynamic Flows," 30th Aerospace Sciences Meeting and Exhibit, AIAA Paper No. 92-0439, January 1992.

[20]Boyd, Jr., D. D., "HART-II Acoustic Predictions using a Coupled CFD/CSD Method," AHS International 65th Forum and Technology Display, May 2009.

[21]Lockard, D. and Casper, J., "Permeable Surface Corrections for Ffowcs Williams and Hawkings Integrals," 11th AIAA/CEAS Aeroacoustics Conference, AIAA Paper No. 2005-2995, May 2005.

[22]Mendez, S., Shoeybi, M., Lele, S. K., and Moin, P., "On the Use of the Ffowcs Williams-Hawkings Equation to Predict Far-Field Jet Noise from Large-Eddy Simulations," *International Journal of Aeroacoustics*, Vol. 12, No. 1, 2013, pp. 1–20.

[23]Farassat, F. and Casper, J., "Broadband noise prediction when turbulence simulation is available–Derivation of Formulation 2B and its statistical analysis," *Journal of Sound and Vibration*, Vol. 331, 2012, pp. 2203–2208.

[24]Casper, J. and Farassat, F., "A New Time Domain Formulation for Broadband Noise Predictions," *International Journal of Aeroacoustics*, Vol. 1, No. 3, 2002, pp. 207–240.

[25]Dunn, M. and Tinetti, A., "Aeroacoustic Scattering via the Equivalent Source Method," 10th AIAA/CEAS Aeroacoustics Conference, AIAA Paper No. 2004-2937, May 2004.

[26]Lee, S., Brentner, K. S., and Morris, P. J., "Assessment of Time-Domain Equivalent Source Method for Acoustic Scattering," *AIAA Journal*, Vol. 49, No. 9, 2011, pp. 1897–1906.

[27]Lopes, L. V., Nielsen, E. J., and Diskin, B., "Adjoint-based Aeroacoustic Design Optimization using CFD," To be presented at the 23rd AIAA/CEAS Aeroacoustics Conference, June 2017.

[28]Levenberg, K., "A Method for the Solution of Certain Non-linear Problems in Least Squares," *Quarterly of Applied Mathematics*, Vol. 2, No. 2, 1944, pp. 164–168.

[29]Marquardt, D. W., "An Algorithm for Least-Squares Estimation of Nonlinear Parameters," *Journal of the Society for Industrial and Applied Mathematics*, Vol. 11, No. 2, 1963, pp. 431–441.

[30]Staffman, P. G., "The Velocity of Viscous Vortex Rings," *Studies in Applied Mathematics*, Vol. 49, No. 4, 1970, pp. 371–380.

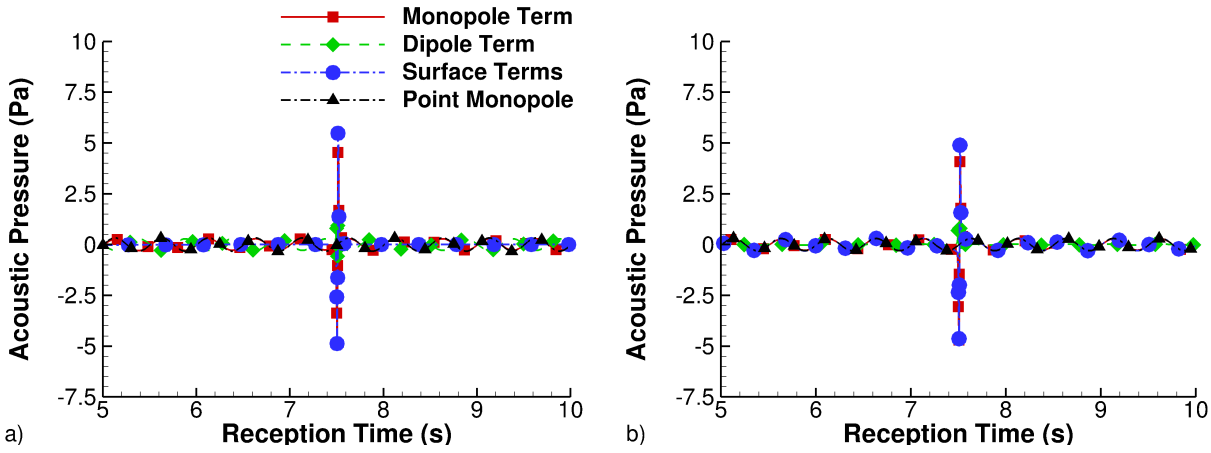

Fig. 18: Acoustic pressure from point monopole and permeable surfaces whose flow properties are defined by the point monopole and vortex ring with core radius a of 0.01 m and forward velocity W of 1 m/s.

Appendix

This section explains the technique employed to determine the flow properties caused by the vortex ring. Lugt (Ref. 14) defined the stream function caused by a vortex ring as a function of vorticity, Γ, shown in Eq. 11. The vorticity can be defined as a function of vortex core diameter, a, ring diameter, R, and convection velocity aligned with the x_3 axis, W_3, shown in Eq. 19 (Ref. 30).

$$\Gamma = W_3 \frac{4\pi R}{\ln\left(8\frac{R}{a}\right) - \frac{1}{4}} \tag{19}$$

This left choice of the vortex core, ring diameter, and convection velocity up to the authors. With the size of the cube-shaped permeable surface in the above study, a vortex ring radius of 1 m was chosen and fixed. A study was then performed on the influence of vortex core radius and convection velocity. Figures 19(a), (c), and (e) (left hand column) show the induced velocity field given $a = 1$ m, $a = 0.1$ m, and $a = 0.01$ m, respectively, with convection velocity fixed at 1 m/s. Two things were observed: 1) near the core, the velocity was unrealistically large, especially for large vortex core diameters[4], shown in Fig. 19, and 2) small vortex core diameters led to very large, very sharp acoustic pressure. The second observation is shown in Fig 18, where the noise caused by the point monopole is compared to that of a vortex ring with vortex core radius of $a = 0.01$ m. Comparison between the vortex ring and point monopole became difficult due to the nature of the pulse caused by the vortex ring.

To overcome these issues, a large vortex core size was chosen, $a = 1$ m, but required an attenuation near the core of the vortex ring. The flow velocities were attenuated inside the core using an attenuation factor, α, that varied with the scaled radius, r/a. This was done by first determining the coordinates of the sampling location in the vortex ring coordinates, denoted with (r, z, Φ), to the vortex core coordinates, denoted as (r_{VC}, z_{VC}, Φ_{VC}), as shown in Eq. 20. A line was then drawn to connect the core of the vortex ring through the sample location. The intersection of this line with the outer edge of the vortex core was then found and is denoted as (r_e, z_e, Φ_e), shown in Eq. 21.

$$\Phi_{\mathrm{VC}} = \mathrm{atan2}(z, r-R), \qquad r_{\mathrm{VC}} = \sqrt{(r-R)^2 - z^2} \tag{20}$$

$$z_e = a\sin\Phi_{\mathrm{VC}}, \qquad r_e = R + a\cos(\Phi_{\mathrm{VC}}) \tag{21}$$

The flow velocities at the edge, $\boldsymbol{u}_e = \boldsymbol{u}(r_e, z_e)$, and core, $\boldsymbol{u}_0 = \boldsymbol{u}(R, 0)$, were then used to determine a baseline velocity, $\boldsymbol{u}_b$, using Eq. 22. The attenuation factor, α, was then determined by a Gaussian fit between the center of the core and the outer edge of the core, as shown in Eq. 23. The application of the attenuation factor to the flow velocity, $\boldsymbol{u} = \boldsymbol{u}(r, z)$, to calculate attenuated velocity, $\boldsymbol{v}$ (Eq. 24), is shown in Figs. 19(b), (d), (f) (right hand column).

$$\boldsymbol{u}_b = \boldsymbol{u}_0 + (\boldsymbol{u}_e - \boldsymbol{u}_0)\sqrt{r_{\mathrm{VR}}/a} \tag{22}$$

$$\alpha = \frac{r_{\mathrm{VC}}}{a}\left(1 - \exp\left\{-\frac{(r_{\mathrm{VC}}/a)^2}{0.005}\right\}\right)^3 \tag{23}$$

$$\boldsymbol{v} = \boldsymbol{u}_b + \alpha(\boldsymbol{u} - \boldsymbol{u}_b) \tag{24}$$

A sweep of different convection velocities was also performed to study the influence of $\boldsymbol{W}$ on the induced flow field. Three calculations were performed for $\boldsymbol{W}$ of 0.5, 1, and 5 m/s; this is shown in Fig. 20. The strength of the vortex field is strongly dependent on the choice of $\boldsymbol{W}$.

[4] Lugt stated that at the core the velocity would go to infinity. The authors found that this was not the case. The velocity would go to a very large and unrealistic value but then quickly, but smoothly, to zero at the core.

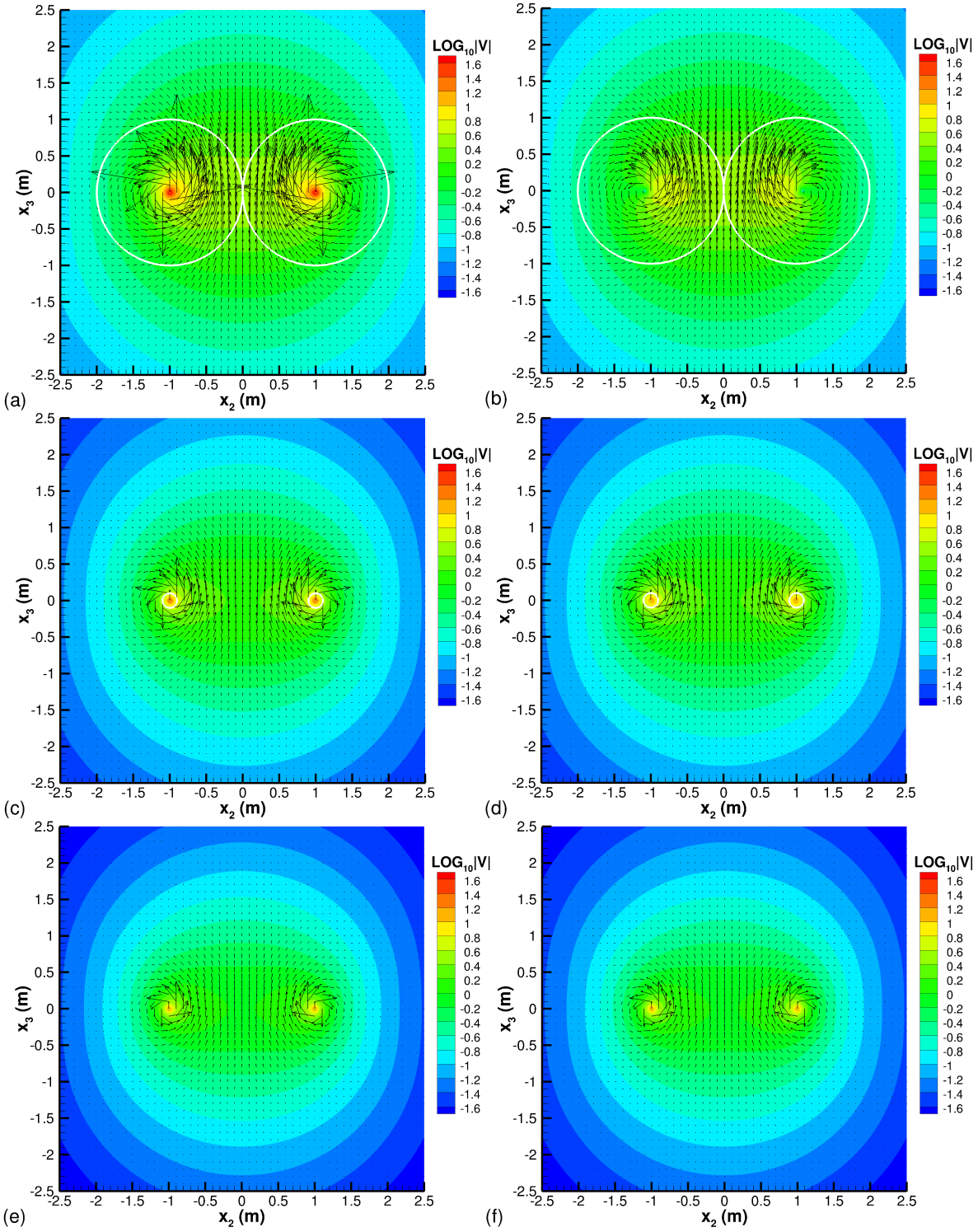

Fig. 19: Flow field induced by vortex ring as a function of core radius. Motion of vortex is aligned with positive x_3 axis; plane centered at origin and normal to x_1 axis. (a) $a = 1$ m unattenuated, (b) $a = 1$ m, attenuated, (c) $a = 0.1$ m, unattenuated, (d) $a = 0.1$ m, attenuated, (e) $a = 0.01$ m, unattenuated, (f) $a = 0.01$ m, attenuated. $W_3 = 1$ m/s for all cases; core size shown as white line and is excluded from Figs. (e) and (f) (too small to be visible).

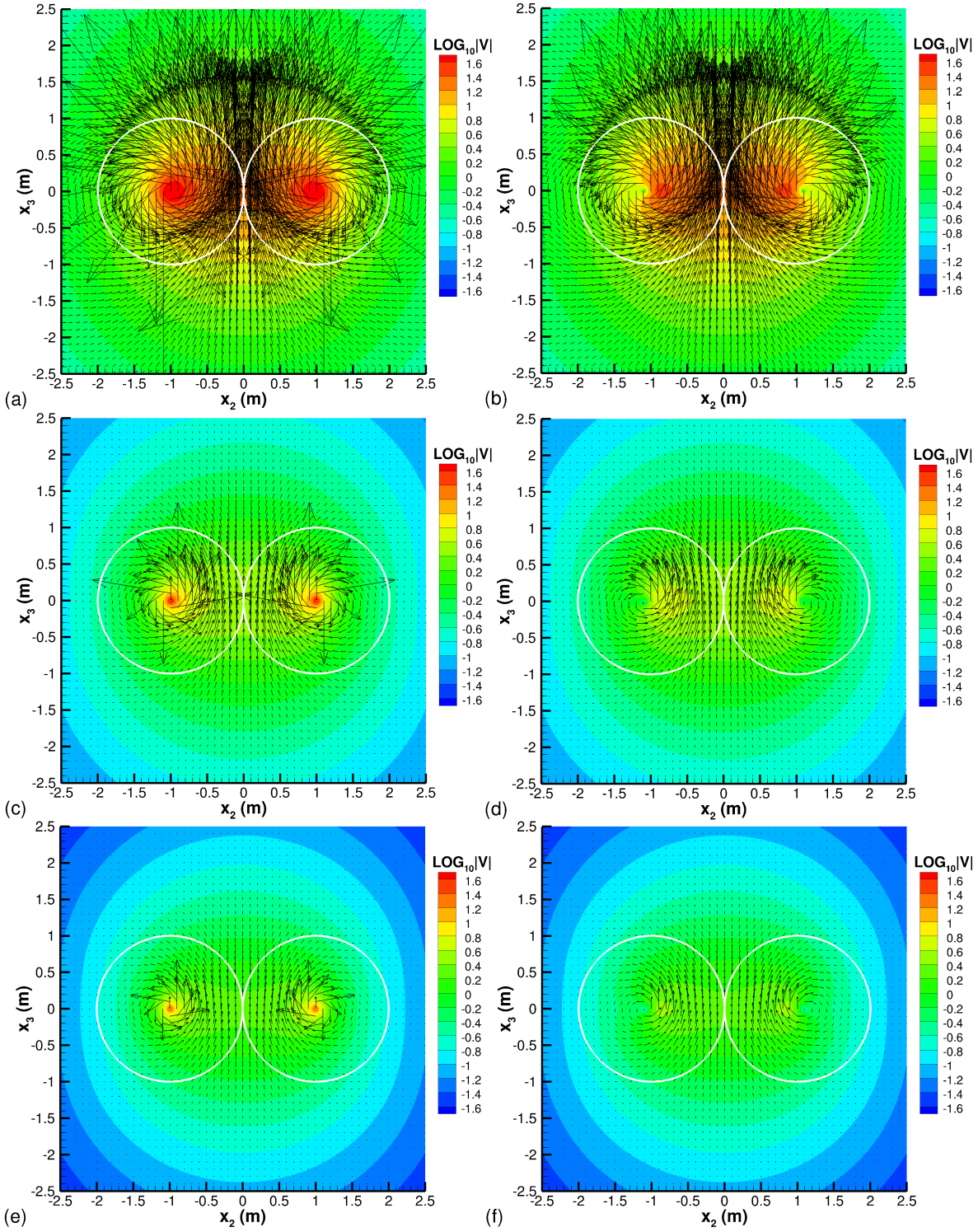

Fig. 20: Flow field induced by vortex ring as a function of convection velocity. Motion of vortex is aligned with positive x_3 axis; plane centered at origin and normal to x_1 axis. (a) $W_3 = 5$ m/s unattenuated, (b) $W_3 = 5$ m/s, attenuated, (c) $W_3 = 1$ m/s, unattenuated, (d) $W_3 = 1$ m/s, attenuated, (e) $W_3 = 0.1$ m/s, unattenuated, (f) $W_3 = 0.1$ m/s, attenuated. $a = 1$ m for all cases; core size shown as white line.